Received: 4 November 2021 | Revised: 16 January 2023 | Accepted: 29 March 2023

DOI: 10.1002/nla.2500

RESEARCH ARTICLE

WILEY

A closed-form multigrid smoothing factor for an additive Vanka-type smoother applied to the Poisson equation

Chen Greif | **Yunhui He**

Department of Computer Science, The University of British Columbia, Vancouver, British Columbia, Canada

Correspondence
Yunhui He, Department of Computer Science, The University of British Columbia, Vancouver, BC, Canada.
Email: yunhui.he@ubc.ca

Funding information
Natural Sciences and Engineering Research Council of Canada

Abstract

We consider an additive Vanka-type smoother for the Poisson equation discretized by the standard finite difference centered scheme. Using local Fourier analysis, we derive analytical formulas for the optimal smoothing factors for vertex-wise and element-wise Vanka smoothers. In one dimension the element-wise Vanka smoother is equivalent to the scaled mass operator obtained from the linear finite element method and in two dimensions the element-wise Vanka smoother is equivalent to the scaled mass operator discretized by bilinear finite element method plus a scaled identity operator. Based on these findings, the mass matrix obtained from finite element method can be used as a smoother for the Poisson equation, and the resulting mass-based relaxation scheme yields small smoothing factors in one, two, and three dimensions, while avoiding the need to compute an inverse of a matrix. Our analysis may help better understand the smoothing properties of additive Vanka approaches and develop fast solvers for numerical solutions of other partial differential equations.

KEYWORDS

additive Vanka-type smoother, finite difference method, local Fourier analysis, mass matrix, multigrid, smoothing factor

1 | INTRODUCTION

Consider the Poisson equation in one dimension (1D), two dimensions (2D), and three dimensions (3D):

$$-\Delta u = f, \tag{1}$$

where u and f are functions in the corresponding number of spatial variables. The function f is assumed to be sufficiently smooth so that finite-difference discretizations of u provide effective approximations of the solution. The differential operator Δ stands for the Laplacian: $\Delta \equiv \frac{d^2}{dx^2}$ in 1D, $\Delta \equiv \frac{\partial^2}{\partial x^2} + \frac{\partial^2}{\partial y^2}$ in 2D, and $\Delta \equiv \frac{\partial^2}{\partial x^2} + \frac{\partial^2}{\partial y^2} + \frac{\partial^2}{\partial z^2}$ in 3D. We assume a uniform mesh discretization with meshsize h.

We apply the standard three, five, and seven-point finite difference discretizations for the Laplacian. For 1D and 2D the corresponding stencils are given by

$$A_h = \frac{1}{h^2}\begin{bmatrix} -1 & 2 & -1 \end{bmatrix}, \tag{2}$$

and

$$A_h = \frac{1}{h^2}\begin{bmatrix} & -1 & \\ -1 & 4 & -1 \\ & -1 & \end{bmatrix}, \tag{3}$$

respectively. For 3D stencil (3) extends straightforwardly in a third dimension, with the value at its center being 6.

Let us denote the corresponding linear system by

$$A_h u_h = b_h. \tag{4}$$

The numerical solution of (4) is one of the most extensively explored topics in the numerical linear algebra literature. The discrete Laplacian A_h is a symmetric positive definite M-matrix, its eigenvalues are explicitly known, and it is used as a primary benchmark problem for the development of fast solvers. When the problem is very large, iterative solvers may be preferred over direct solvers, and may be further accelerated by parallelizing the computation.

One of the most efficient methods for solving (4) is *multigrid*.[1,2] There are several studies of smoothers for multigrid for the Poisson equation, such as red–black Gauss Seidel (GS-RB),[3,4] red–black SOR,[5] lexicographic Gauss–Seidel,[6] acceleration of five-point red–black Gauss–Seidel,[7] to mention just a few papers.

The choice of additive Vanka as relaxation scheme is suitable for parallel computing. Vanka-type smoothers have been applied to the Navier–Stokes equations,[8-10] the Poisson equation using continuous and discontinuous finite elements methods,[11] the Stokes equations with finite element methods,[12,13] poroelasticity equations[14] in monolithic multigrid, and other problems. A restricted additive Vanka for Stokes using $Q_1 - Q_1$ discretizations[15] has demonstrated its competitiveness with the multiplicative Vanka smoother. Nonoverlapping block smoothing using different patches has been applied to the Stokes equations discretized by the marker-and-cell scheme.[16] Multiplicative Vanka smoothers in combination with multigrid methods have been considered by several authors.[17-19] Vanka-type relaxation has been used in several contexts.[8,20,21] A two-grid analysis for Vanka smoothing is discussed for the mixed finite element discretization of the Poisson equation.[22] Weighted max-norm bounds are obtained for algebraic additive Schwarz iterations[23] where the coefficient matrix is an M-matrix. Different Vanka-type smoothers are presented[24] for the Stokes equations. Vanka smoothers are used in the context of discontinuous Galerkin discretization of the Stokes equations.[20] Vanka-like multigrid smoothers in the context of finite element simulations for elasticity equations have also been explored.[25] Vanka-based multigrid relaxation methods for incompressible fluid dynamics has been studied,[26] compared with Braess-Sarazin smoother. Convergence properties and numerical examples of Vanka-type smoothers for solving Stokes and Navier–Stokes problems have been studied[9] under suitable conditions. Recently, a scalable and robust vertex-star patch relaxation has been proposed, applicable to higher polynomial degrees of finite element methods.[27]

Solvers for the Poisson equation often form the first step for designing fast solvers for more complex problems, such as the Stokes equations, and Navier–Stokes equations. We therefore believe that the findings in this work can be potentially useful for designing fast numerical methods for these complex problems.

In the literature, Vanka-type relaxation schemes demonstrate their high efficiency in a multigrid setting, but there seems no theoretical analysis for the convergence speed even for the simple Poisson equation. In this work we take steps towards closing this gap by considering the additive Vanka relaxation for the Poisson equation, and exploring stencils for the Vanka patches. The simplicity of the Poisson equation allows us to make a distinct contribution from an analytical point of view, because we are able to derive explicit stencils. Doing so, we find that the mass matrix (stencil) is related to a type of a Vanka stencil, and we further derive the optimal smoothing factor using the mass matrix as a smoother. This is possible only for the sufficiently-simple structure that the Laplacian offers, and in this regard the paper offers new insights. As far as we know, no previous articles in the literature provide an analysis based on the stencil of a Vanka smoother, nor do they consider the mass matrix as a specific potential smoother within this type.

This work further extends work on Vanka patches that was introduced for hybridized and embedded discontinuous Galerkin methods.[11] Here, we find the corresponding stencils for the Vanka operators, and show that they are closely related to the scaled mass matrix obtained from the finite element method. Based on this discovery, we propose the mass-based relaxation scheme, which yields rapid convergence. This mass-based relaxation is very simple: the computational cost is only matrix-vector product and there is no need to solve the subproblems needed in an additive Vanka setting. Another advantage of the mass matrices obtained from (bi)linear elements is sparsity.

The remainder of this article is organized as follows. In Section 2, we introduce the two types of additive Vanka smoothers for the Poisson equation. In Section 3, we present our theoretical analysis of optimal smoothing factors in 1D and 2D. Based on our analysis we also propose a mass-based smoother for the three-dimensional problem, where the mass matrix is obtained from the trilinear finite element method. In Section 4, we numerically validate our analytical observations and present an LFA two-grid convergence factor and multigrid performance. Finally, in Section 5 we discuss our findings and draw some conclusions.

2 | VANKA-TYPE SMOOTHER

We are interested in exploring the structure of additive Vanka-type smoothers for solving the linear system (4) using multigrid. In general, this type can be thought of as related to the family of block Jacobi smoothers, which are suitable for parallel computation and are typically highly efficient within the context of multigrid smoothing.

Let the degrees of freedom (DoFs) of u_h be the set Υ such that $\Upsilon = \bigcup_{i=1}^{N} \Upsilon_i$. V_i is a restriction operator that maps the vector u_h onto the vector in Υ_i. Define

$$A_i = V_i A_h V_i^T.$$

Then, we update current approximation u^j by a single Vanka relaxation given by:

$$A_i \delta u_i = V_i (b_h - A_h u^j), \qquad i = 1, \dots, N,$$

and

$$u^{j+1} = u^j + \sum_{i=1}^{N} V_i^T W_i \delta u_i.$$

A single iteration of the Vanka smoother can be represented as

$$M = \sum_{i=1}^{N} V_i^T W_i A_i^{-1} V_i, \tag{5}$$

where the weighting matrix $W = W_i$ is given by the natural weights of the overlapping block decomposition. Each diagonal entry is equal to the reciprocal of the number of patches that the corresponding degree of freedom appears in. We refer to M the *Vanka operator*.

For a single additive Vanka relaxation process, the relaxation error operator is given by

$$S = I - \omega M A_h. \tag{6}$$

A key factor is the choice of the patch, that is, the $\{\Upsilon_i\}$. We study two patches,[11] which are selected based on simple geometric considerations and a structural similarity to the five-point Laplacian stencil, shown in Figure 1. We refer to the left patch in Figure 1 as an *element-wise patch* and the right one as a *vertex-wise patch*, and denote the corresponding relaxation error operators defined in (6) as S_e and S_v, respectively. We denote the additive smoothers by AS-e and AS-v, respectively. The circles indicate the number of DoFs in one patch Υ_i. This means that the resulting subproblem is associated with a small matrix A_i whose size is 4×4 or 5×5. In the remainder of this work, for simplicity and clarity we use subscripts e and v to distinguish between the corresponding operators for element-wise Vanka and vertex-wise Vanka, respectively.

3 | LOCAL FOURIER ANALYSIS

Local Fourier analysis (LFA)[28,29] is a useful tool for predicting and analyzing the convergence behavior of multigrid and other numerical algorithms. In this section, we use LFA to study the proposed Vanka-type smoothers.

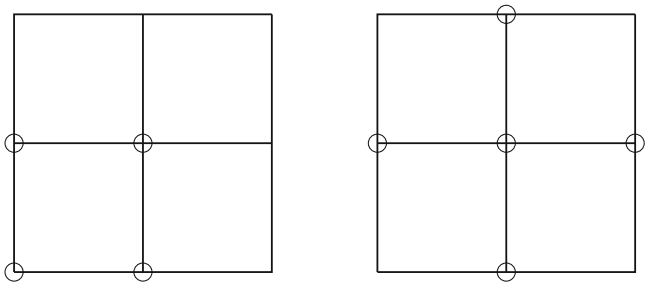

FIGURE 1 Left: Element-wise patch. Right: Vertex-wise patch.

LFA works under the assumption that the smoothing process reduces high frequencies and leaves low frequencies unchanged.[28] The LFA smoothing factor typically offers a rather sharp bound on the actual two-grid performance. We proceed by defining the high and low frequencies for standard coarsening ($H = 2h$) as follows:

$$\boldsymbol{\theta} \in T^{\text{low}} = \left[-\frac{\pi}{2}, \frac{\pi}{2}\right)^d, \quad \boldsymbol{\theta} \in T^{\text{high}} = \left[-\frac{\pi}{2}, \frac{3\pi}{2}\right)^d \setminus \left[-\frac{\pi}{2}, \frac{\pi}{2}\right)^d,$$

where d is the dimension of the underlying problem.

Definition 1. Assume that a scalar operator L_h is defined by the stencil $[s_\kappa]$, which acts on a grid function $w_h(x)$ given by[28]

$$L_h w_h(x) = \sum_{\kappa \in \Xi} s_\kappa w_h(x + \kappa h),$$

where Ξ is a finite index set. Then, the symbol of L_h is defined as

$$\widetilde{L}_h = \sum_{\kappa \in \Xi} e^{\imath \kappa \boldsymbol{\theta}}, \quad \imath^2 = -1.$$

Definition 2. Let S be the relaxation error operator. Then, the corresponding LFA smoothing factor for S is given by

$$\mu(\omega) = \max_{\boldsymbol{\theta} \in T^{\text{high}}} \left\{ \rho(\widetilde{S}(\boldsymbol{\theta}, \omega)) \right\}, \tag{7}$$

where $\widetilde{S}(\boldsymbol{\theta}, \omega)$ is the symbol of S, ω is algorithmic parameter, and $\rho(\widetilde{S}(\boldsymbol{\theta}, \omega))$ denotes the spectral radius of the matrix $\widetilde{S}(\boldsymbol{\theta}, \omega)$.

Note that the LFA smoothing factor μ is a function of ω. Often, one can minimize (7) with respect to ω to obtain fast convergence speed. We define the optimal smoothing factor as

$$\mu_{\text{opt}} = \min_{\omega} \mu. \tag{8}$$

In this work, the symbol $\widetilde{S}$ for the Laplacian considered is a scalar, so the spectral radius is reduced to the maximum of a scalar function. In the following, we use LFA to identify the optimal smoothing factor for the additive Vanka-type relaxation schemes and explore the structure of the Vanka operator M defined in (5). Before providing our detailed analysis of the smoothing factor for different relaxation schemes, we summarize our results in Table 1. The table provides a review of quantitative results of additive Vanka smoothers, and for comparison we include results for the standard point-wise damped Jacobi smoother.

Note that a general form of the symbol of additive Vanka operator for the Stokes equations is available,[12] which gives $\widetilde{M} = \widetilde{V}^T \widetilde{W} \Phi^T A_i^{-1} \Phi \widetilde{V}$, where Φ is called the *relative Fourier matrix*. Here, we can directly apply the formula of $\widetilde{M}$ to our additive Vanka operator.[12]

TABLE 1 Optimal LFA smoothing factors in 1D and 2D.

Smoother	Jacobi	AS-e	AS-v
1D			
ω_{opt}	2/3	12/17	81/104
μ_{opt}	0.333	0.059	0.039
2D			
ω_{opt}	4/5	24/25	20/23
μ_{opt}	0.600	0.280	0.391

3.1 | Symbols of Vanka smoothers in 1D

In this section, we first consider the symbol of the element-wise smoother, then the vertex-wise smoother for the Laplacian in 1D. We discuss the optimal smoothing factor for each case and derive the corresponding stencil for the Vanka operator.

3.1.1 | Element-wise Vanka patch in 1D

Using Definition 1 it can easily be shown that the symbol of A_h, see (2), is given by

$$\widetilde{A}_h = \frac{1}{h^2} 2(1 - \cos\theta). \tag{9}$$

Moreover, for the element-wise patch the subproblem matrix is

$$A_i = \frac{1}{h^2} \begin{pmatrix} 2 & -1 \\ -1 & 2 \end{pmatrix}.$$

The relative Fourier matrix[12] Φ is

$$\Phi_e = \begin{pmatrix} 1 & 0 \\ 0 & e^{\imath\theta} \end{pmatrix}.$$

Then, the symbol of M_e is given by $\widetilde{M}_e = \widetilde{V}^T \widetilde{W} \Phi_e^T A_i^{-1} \Phi_e \widetilde{V}$, where

$$\widetilde{V} = \begin{pmatrix} 1 \\ 1 \end{pmatrix}, \quad \widetilde{W} = \frac{1}{2} \begin{pmatrix} 1 & 0 \\ 0 & 1 \end{pmatrix}, \quad A_i^{-1} = \frac{h^2}{3} \begin{pmatrix} 2 & 1 \\ 1 & 2 \end{pmatrix}.$$

Based on the above formulas, we obtain

$$\widetilde{M}_e = \frac{h^2}{6}(4 + e^{\imath\theta} + e^{-\imath\theta}). \tag{10}$$

Formula (10) indicates that the element-wise Vanka patch corresponds to the stencil

$$M_e = \frac{h^2}{6} \begin{bmatrix} 1 & 4 & 1 \end{bmatrix}. \tag{11}$$

Recall that the mass stencil in 1D using linear finite elements is given by Matt[30]

$$M_{fe} = \frac{h}{6} \begin{bmatrix} 1 & 4 & 1 \end{bmatrix}. \tag{12}$$

This means that the element-wise Vanka operator is equivalent to a scaled mass matrix obtained from the linear finite element method, $M_e = hM_{fe}$.

Next, we give the optimal smoothing factor for the element-wise Vanka relaxation scheme.

Theorem 1. The optimal smoothing factor of S_e for the vertex-wise Vanka in 1D is

$$\mu_{e,\text{opt}} = \min_{\omega} \max_{\theta \in T^{\text{high}}} |1 - \omega \widetilde{M}_e \widetilde{A}_h| = \frac{1}{17} \approx 0.059, \tag{13}$$

where the minimum is uniquely achieved at $\omega = \omega_{\text{opt}} = \frac{12}{17} \approx 0.706$.

Proof. When $\theta \in T^{\text{high}} = [\frac{\pi}{2}, \frac{3\pi}{2}]$,

$$\widetilde{M}_e \widetilde{A}_h = \frac{2}{3}(2 - \cos\theta - \cos^2\theta) \in \left[\frac{4}{3}, \frac{3}{2}\right].$$

Thus,

$$\mu(\omega) = \max |1 - \omega \widetilde{M}_e \widetilde{A}_h| = \max \left\{ \left|1 - \omega \frac{4}{3}\right|, \left|1 - \omega \frac{3}{2}\right| \right\}.$$

To minimize $\mu(\omega)$, we require

$$\left|1 - \omega \frac{4}{3}\right| = \left|1 - \omega \frac{3}{2}\right|,$$

which gives $\omega = \frac{2}{4/3+3/2} = \frac{12}{17}$. Then, $\mu_{\text{opt}} = 1 - \frac{2}{4/3+3/2}\frac{4}{3} = \frac{1}{17}$. ∎

It is well known that the optimal smoothing factor for damped Jacobi relaxation for the Laplacian in 1D (with $\omega = \frac{2}{3}$) is $\frac{1}{3} \approx 0.333 \gg 0.059$. This suggests that using the additive Vanka smoother for multigrid achieves much faster convergence.

3.1.2 | Vertex-wise Vanka patch in 1D

We now consider the vertex-wise patch. The subproblem matrix is

$$A_i = \frac{1}{h^2}\begin{pmatrix} 2 & -1 & 0 \\ -1 & 2 & -1 \\ 0 & -1 & 2 \end{pmatrix}.$$

The relative Fourier matrix[12] Φ is

$$\Phi_v = \begin{pmatrix} e^{-\iota\theta} & 0 & 0 \\ 0 & 1 & 0 \\ 0 & 0 & e^{\iota\theta} \end{pmatrix}.$$

Then, the symbol of M_v is given by $\widetilde{M}_v = \widetilde{V}^T \widetilde{W} \Phi_v^T A_i^{-1} \Phi_v \widetilde{V}$, where

$$\widetilde{V} = \begin{pmatrix} 1 \\ 1 \\ 1 \end{pmatrix}, \quad \widetilde{W} = \frac{1}{3}\begin{pmatrix} 1 & 0 & 0 \\ 0 & 1 & 0 \\ 0 & 0 & 1 \end{pmatrix}, \quad A_i^{-1} = \frac{h^2}{4}\begin{pmatrix} 3 & 2 & 1 \\ 2 & 4 & 2 \\ 1 & 2 & 3 \end{pmatrix}.$$

Using the above formulas, we have

$$\widetilde{M}_v = \widetilde{V}^T \widetilde{W} \Phi_v^T A_i^{-1} \Phi_v \widetilde{V} = \frac{h^2}{12}(10 + 4e^{\imath\theta} + 4e^{-\imath\theta} + e^{\imath 2\theta} + e^{-\imath 2\theta}). \tag{14}$$

Based on (14), the stencil of M_v is

$$M_v = \frac{h^2}{12}\begin{bmatrix} 1 & 4 & 10 & 4 & 1 \end{bmatrix}. \tag{15}$$

Compared with (11), the vertex-wise Vanka uses a wider stencil.

Theorem 2. The optimal smoothing factor of S_v for the vertex-wise Vanka in 1D is

$$\mu_{v,\text{opt}} = \min_{\omega} \max_{\theta \in T^{\text{high}}} |1 - \omega \widetilde{M}_v \widetilde{A}_h| = \frac{1}{26} \approx 0.039, \tag{16}$$

where the minimum is uniquely achieved at $\omega = \omega_{\text{opt}} = \frac{81}{104} \approx 0.779$.

Proof. From (9) and (14), we have

$$\begin{aligned} \widetilde{M}_v \widetilde{A}_h &= \frac{1}{3}(1 - \cos\theta)\,(5 + 4\cos\theta + \cos(2\theta))\,, \\ &= \frac{2}{3}(1 - \cos\theta)(2 + 2\cos\theta + \cos^2\theta), \\ &= \frac{2}{3}(1 - \cos\theta)\left((\cos\theta + 1)^2 + 1\right). \end{aligned}$$

Note that when $\theta \in T^{\text{high}} = [\frac{\pi}{2}, \frac{3\pi}{2}]$, $\cos\theta \in [-1, 0]$. Let $g(x) = \frac{2}{3}(1 - x)\left((x + 1)^2 + 1\right)$, where $x = \cos\theta \in [-1, 0]$. To identify the range of $g(x)$, we first compute its derivative:

$$g'(x) = \frac{-2}{3}x(3x + 2) < 0, \quad \text{for } x \in [-1, 0].$$

It follows that

$$\left(\frac{10}{9}\right)^2 = g(-2/3) \le g(x) \le g(0) = g(1) = \frac{4}{3}.$$

That is, $\widetilde{M}_v \widetilde{A}_h \in [(\frac{10}{9})^2, \frac{4}{3}]$ for $\theta \in T^{\text{high}}$. To minimize $\mu(\omega)$, we require $\omega = \frac{2}{4/3 + (10/9)^2} = \frac{81}{104}$. Then, it follows that $\mu_{\text{opt}} = 1 - \frac{2}{4/3 + (10/9)^2}(\frac{10}{9})^2 = \frac{1}{26}$. ∎

Again, the optimal smoothing factor for vertex-wise Vanka is significantly smaller (and hence better) than that of the damped Jacobi relaxation scheme.

3.2 | Symbols of Vanka smoothers in 2D

Similarly to previous subsection, we first consider the analytical symbol for the element-wise patch, then for the vertex-wise patch for the Laplacian in 2D.

3.2.1 | Element-wise Vanka patch in 2D

The symbol of Laplace operator discretized by five-point stencil, see (3), is

$$\widetilde{A}_h = \frac{1}{h^2}(4 - e^{\imath\theta_1} - e^{\imath\theta_2} - e^{-\imath\theta_1} - e^{-\imath\theta_2}) = \frac{1}{h^2}\,(4 - 2\cos\theta_1 - 2\cos\theta_2)\,. \tag{17}$$

For the element-wise patch, the relative Fourier matrix[12] Φ is

$$\Phi_e = \begin{pmatrix} 1 & 0 & 0 & 0 \\ 0 & e^{\imath\theta_1} & 0 & 0 \\ 0 & 0 & e^{\imath\theta_2} & 0 \\ 0 & 0 & 0 & e^{\imath(\theta_1+\theta_2)} \end{pmatrix}.$$

Then, the symbol of M_e is given by $\widetilde{M}_e = \widetilde{V}^T\widetilde{W}\Phi_e^T A_i^{-1}\Phi_e\widetilde{V}$, where

$$\widetilde{W} = \frac{1}{4}\begin{pmatrix} 1 & 0 & 0 & 0 \\ 0 & 1 & 0 & 0 \\ 0 & 0 & 1 & 0 \\ 0 & 0 & 0 & 1 \end{pmatrix}, \quad \widetilde{V} = \begin{pmatrix} 1 \\ 1 \\ 1 \\ 1 \end{pmatrix}, \quad A_i = \frac{1}{h^2}\begin{pmatrix} 4 & -1 & -1 & 0 \\ -1 & 4 & 0 & -1 \\ -1 & 0 & 4 & -1 \\ 0 & -1 & -1 & 4 \end{pmatrix}.$$

We have

$$A_i^{-1} = h^2\begin{pmatrix} 7/24 & 1/12 & 1/12 & 1/24 \\ 1/12 & 7/24 & 1/24 & 1/12 \\ 1/12 & 1/24 & 7/24 & 1/12 \\ 1/24 & 1/12 & 1/12 & 7/24 \end{pmatrix},$$

and it follows that

$$\begin{aligned} \widetilde{M}_e &= \widetilde{V}^T\widetilde{W}\Phi_e^T A_i^{-1}\Phi_e\widetilde{V}, \\ &= \frac{h^2}{96}\left(28 + 4(e^{\imath\theta_1} + e^{-\imath\theta_1} + e^{\imath\theta_2} + e^{-\imath\theta_2}) + e^{\imath(\theta_1+\theta_2)} + e^{-\imath(\theta_1+\theta_2)} + (e^{\imath\theta_1}e^{-\imath\theta_2} + e^{-\imath\theta_1}e^{\imath\theta_2})\right), \\ &= \frac{h^2}{24}\left(7 + 2(\cos\theta_1 + \cos\theta_2) + \cos\theta_1\cos\theta_2\right). \end{aligned} \tag{18}$$

Based on the symbol of M_e, we obtain the stencil of M_e,

$$M_e = \frac{h^2}{96}\begin{bmatrix} 1 & 4 & 1 \\ 4 & 28 & 4 \\ 1 & 4 & 1 \end{bmatrix}. \tag{19}$$

Recall that the mass matrix stencil using bilinear finite elements is[30]

$$M_{fe} = \frac{h^2}{36}\begin{bmatrix} 1 & 4 & 1 \\ 4 & 16 & 4 \\ 1 & 4 & 1 \end{bmatrix}. \tag{20}$$

Now, we can make a connection between M_e and M_{fe}:

$$M_e = \frac{3}{8}M_{fe} + \frac{h^2}{8}\mathcal{I}, \tag{21}$$

where

$$\mathcal{I} = \begin{bmatrix} 0 & 0 & 0 \\ 0 & 1 & 0 \\ 0 & 0 & 0 \end{bmatrix}. \tag{22}$$

Next, we give the optimal smoothing factor for the element-wise Vanka relaxation in 2D.

Theorem 3. The optimal smoothing factor of S_e for the element-wise Vanka relaxation in 2D is given by

$$\mu_{e,\text{opt}} = \min_{\omega} \max_{\theta \in T^{\text{high}}} |1 - \omega \widetilde{M}_e \widetilde{A}_h| = \frac{7}{25} \approx 0.280, \tag{23}$$

where the minimum is uniquely achieved at $\omega = \omega_{\text{opt}} = \frac{24}{25} \approx 0.960$.

Proof. From (17) and (18), we have

$$\begin{aligned}
\widetilde{M}_e \widetilde{A}_h &= \frac{1}{24} (7 + 2(\cos\theta_1 + \cos\theta_2) + \cos\theta_1 \cos\theta_2)(4 - 2\cos\theta_1 - 2\cos\theta_2), \\
&= \frac{1}{12} (7 + 2(\cos\theta_1 + \cos\theta_2) + \cos\theta_1 \cos\theta_2)(2 - (\cos\theta_1 + \cos\theta_2)), \\
&= \frac{1}{12} (7 + 2(\eta_1 + \eta_2) + \eta_1\eta_2)(2 - \eta_1 - \eta_2),
\end{aligned}$$

where $\eta_1 = \cos\theta_1, \eta_2 = \cos\theta_2$. Let

$$g(\eta_1, \eta_2) = \frac{1}{12} (7 + 2(\eta_1 + \eta_2) + \eta_1\eta_2)(2 - \eta_1 - \eta_2).$$

We have $(\eta_1, \eta_2) \in [-1, -1]^2 =: \Omega$ and $g(\eta_1, \eta_2)$ is continuous in Ω. By the Extreme Value Theorem, g achieves its extreme values at the boundary of Ω or at points where its derivatives are zeros. We first consider the derivatives,

$$\begin{aligned}
g_{\eta_1} &= \frac{1}{12}(-3 - 4\eta_1 - 2\eta_1\eta_2 - \eta_2^2 - 2\eta_2), \\
g_{\eta_2} &= \frac{1}{12}(-3 - 4\eta_2 - 2\eta_1\eta_2 - \eta_2^2 - 2\eta_1).
\end{aligned}$$

Solving $g_{\eta_1} = g_{\eta_1} = 0$ gives $\eta_1 = \eta_2 = -1$. Thus, $g(-1, -1) = \frac{4}{3}$ is a possible global extreme value.

Next, we compute the extremals of $g(\eta_1, \eta_2)$ at the boundary Ω. Due to the symmetry of g, we only need to consider the following two cases.

- **Case 1**: $\eta_1 = -1$ and $\eta_2 \in [-1, 1]$. We have

$$g(-1, \eta_2) = \frac{1}{12}(5 + \eta_2)(3 - \eta_2).$$

  Thus,

$$1 = g(-1, 1) \le g(-1, \eta_2) \le g(-1, -1) = \frac{4}{3}.$$

- **Case 2**: $\eta_1 = 1$ and $\eta_2 \in [-1, 1]$. We have

$$g(1, \eta_2) = \frac{1}{4}(3 + \eta_2)(1 - \eta_2).$$

  Thus,

$$0 = g(1, 1) \le g(1, \eta_2) \le g(1, -1) = 1.$$

If we restrict $(\theta_1, \theta_2) \in T^{\text{high}}$, we find that the maximum and minimum of $\widetilde{M}_e\widetilde{A}_h = g(\eta_1, \eta_2)$ are given by

$$g(-1,-1) = \frac{4}{3}, \quad g(1,0) = \frac{3}{4}, \tag{24}$$

respectively. It follows that $\omega_{\text{opt}} = \frac{2}{3/4+4/3} = \frac{24}{25}$ and $\mu_{e,\text{opt}} = 1 - \frac{2}{4/3+3/4}\frac{3}{4} = \frac{7}{25}$. ∎

It is well known that the optimal smoothing factor for damped Jacobi relaxation for the Laplacian in 2D is $\frac{3}{5}$ with $\omega = \frac{4}{5}$.[28] This suggests that using the additive Vanka smoother for multigrid method, convergence is faster compared to the damped Jacobi relaxation scheme.

The relationship (21) indicates that the Vanka smoother can be expressed as a linear combination of the identity and the mass matrix obtained from bilinear elements. The scaled identity is related to damped Jacobi smoothing. It is therefore natural to consider the other term, namely the mass matrix, as a smoother. Let us, then, move to consider the smoothing properties of the mass matrix (20).

Theorem 4. Given the mass stencil M_{fe} in (20) and the relaxation scheme $S_{fe} = I - \omega M_{fe} A_h$, the corresponding optimal smoothing factor is

$$\mu_{fe,\text{opt}} = \min_{\omega} \max_{\boldsymbol{\theta} \in T^{\text{high}}} |1 - \omega \widetilde{M}_{fe}\widetilde{A}_h| = \frac{1}{3} \approx 0.333, \tag{25}$$

where the minimum is uniquely achieved at $\omega = \omega_{opt} = \frac{3}{4}$.

Proof. It can easily be shown that $\widetilde{M}_{fe}\widetilde{A}_h \in \left[\frac{8}{9}, \frac{16}{9}\right]$ for $(\theta_1, \theta_2) \in T^{\text{high}}$. Thus, the optimal ω is $\omega = \frac{2}{8/9+16/9} = \frac{3}{4}$. Then, $\mu_{fe,opt} = 1 - \frac{2}{16/9+8/9}\frac{8}{9} = \frac{1}{3}$. ∎

From Theorem 4, we see that the optimal smoothing factor of 0.333 for the mass-based relaxation is close to the optimal smoothing factor 0.280 for the element-wise Vanka patch, and it is better than 0.391 obtained from the vertex-wise Vanka (30), discussed in the next subsection. Thus, mass matrix could be used as a good smoother for this problem.

3.2.2 | Vertex-wise Vanka patch in 2D

Now, we analyse the smoothing factor for the vertex-wise patch. The relative Fourier matrix[12] Φ is

$$\Phi_v = \begin{pmatrix} e^{-\imath\theta_2} & 0 & 0 & 0 & 0 \\ 0 & e^{-\imath\theta_1} & 0 & 0 & 0 \\ 0 & 0 & 1 & 0 & 0 \\ 0 & 0 & 0 & e^{\imath\theta_1} & 0 \\ 0 & 0 & 0 & 0 & e^{\imath\theta_2} \end{pmatrix}. \tag{26}$$

The symbol of M_v is given by $\widetilde{M}_v = \widetilde{V}^T\widetilde{W}\Phi_v^T A_i^{-1}\Phi_v\widetilde{V}$ with

$$\widetilde{W} = \frac{1}{5}I, \quad \widetilde{V} = \begin{pmatrix} 1 \\ 1 \\ 1 \\ 1 \\ 1 \end{pmatrix}, \quad A_i = \frac{1}{h^2}\begin{pmatrix} 4 & 0 & -1 & 0 & 0 \\ 0 & 4 & -1 & 0 & 0 \\ -1 & -1 & 4 & -1 & -1 \\ 0 & 0 & -1 & 4 & 0 \\ 0 & 0 & -1 & 0 & 4 \end{pmatrix}, \tag{27}$$

where I stands for identity matrix of size 5×5.

It can be shown that

$$A_i^{-1} = h^2 \begin{pmatrix} 13/48 & 1/48 & 1/12 & 1/48 & 1/48 \\ 1/48 & 13/48 & 1/12 & 1/48 & 1/48 \\ 1/12 & 1/12 & 1/3 & 1/12 & 1/12 \\ 1/48 & 1/48 & 1/12 & 13/48 & 1/48 \\ 1/48 & 1/48 & 1/12 & 1/48 & 13/48 \end{pmatrix}. \tag{28}$$

From (26)–(28), we have

$$\begin{aligned} \widetilde{M}_v &= \widetilde{V}^T \widetilde{W} \Phi_v^T A_i^{-1} \Phi_v \widetilde{V}, \\ &= \frac{h^2}{240} \left(8(e^{-\iota\theta_2} + e^{\iota\theta_2} + e^{-\iota\theta_1} + e^{\iota\theta_1}) + 68 + (e^{-\iota\theta_2} + e^{-\iota\theta_1})^2 + (e^{\iota\theta_2} + e^{\iota\theta_1})^2 + 2(e^{-\iota\theta_2} e^{\iota\theta_1} + e^{\iota\theta_2} e^{-\iota\theta_1}) \right), \\ &= \frac{h^2}{240} \left(16(\cos\theta_1 + \cos\theta_2) + 68 + 2\left((\cos\theta_1 + \cos\theta_2)^2 - (\sin\theta_1 + \sin\theta_2)^2 \right) + 4\cos(\theta_1 - \theta_2) \right) \\ &= \frac{h^2}{120} \left((\cos\theta_1 + \cos\theta_2 + 4)^2 + (\cos\theta_1 + \cos\theta_2)^2 + 16 \right). \end{aligned}$$

Based on the symbol of M_v, we can write the corresponding stencil of M_v as follows:

$$M_v = \frac{h^2}{240} \begin{bmatrix} 0 & 0 & 1 & 0 & 0 \\ 0 & 2 & 8 & 2 & 0 \\ 1 & 8 & 68 & 8 & 1 \\ 0 & 2 & 8 & 2 & 0 \\ 0 & 0 & 1 & 0 & 0 \end{bmatrix}. \tag{29}$$

Now, we are able to give the optimal smoothing factor for the vertex-wise Vanka relaxation scheme.

Theorem 5. The optimal smoothing factor of S_v for the vertex-wise Vanka relaxation in 2D is

$$\mu_{\text{opt}} = \min_{\omega} \max_{\theta \in T^{\text{high}}} |1 - \omega \widetilde{M}_v \widetilde{A}_h| = \frac{9}{23} \approx 0.391, \tag{30}$$

where the minimum is uniquely achieved at $\omega = \omega_{opt} = \frac{20}{23} \approx 0.8696$.

Proof. We first compute

$$\begin{aligned} \widetilde{M}_v \widetilde{A}_h &= \frac{1}{120} \left((\cos\theta_1 + \cos\theta_2 + 4)^2 + (\cos\theta_1 + \cos\theta_2)^2 + 16 \right) (4 - 2\cos\theta_1 - 2\cos\theta_2) \\ &= \frac{1}{60} \left((4 + \eta)^2 + \eta^2 + 16 \right) (2 - \eta), \end{aligned}$$

where $\eta = (\cos\theta_1 + \cos\theta_2) \in [-2, 2]$ with $(\theta_1, \theta_2) \in \left[-\frac{\pi}{2}, \frac{3\pi}{2} \right]^2$.

Let $g(\eta) = \frac{1}{60} \left((4 + \eta)^2 + \eta^2 + 16 \right) (2 - \eta)$. We find that

$$g'(\eta) = \frac{1}{30}(-3\eta^2 - 4\eta - 8) < 0, \quad \forall \eta \in \mathbb{R}.$$

This means that $g(\eta)$ is a decreasing function. Thus, for $\eta \in [-2, 2]$, we have

$$0 = g(\eta = 2) \le g(\eta) \le g(\eta = -2) = \frac{8}{5}.$$

This means that $g(\eta) \in [0, \frac{8}{5}]$.

If we restrict $(\theta_1, \theta_2) \in T^{\text{high}}$, then $\eta \in [-2, 1]$. In this situation, we have

$$\frac{7}{10} = g(\eta = 1) \leq g(\eta) \leq g(\eta = -2) = \frac{8}{5}.$$

Since $\widetilde{M}_v \widetilde{A}_h \in [\frac{7}{10}, \frac{8}{5}]$ for $(\theta_1, \theta_2) \in T^{\text{high}}$, we have $\omega_{\text{opt}} = \frac{2}{7/10+8/5} = \frac{20}{23}$ and $\mu_{\text{opt}} = 1 - \frac{20}{23}\frac{7}{10} = \frac{9}{23}$. ∎

Remark 1. Note that in 2D the element-wise Vanka stencil, see (19), uses fewer points than that of vertex-wise Vanka, see (29). However, the corresponding optimal smoothing factor of element-wise Vanka, see (23), is smaller than that of vertex-wise Vanka, see (30), which is different than the case in 1D.

3.3 | Extension to the 3D case

While we do not include a smoothing analysis of Vanka-type solvers for the 3D case, we can still make a few interesting observations. In particular, motivated by our findings on the potential role of the mass matrix for relaxation, we further explore the scaled mass matrix in 3D as a smoother for the Laplacian. Let

$$M = h^{-4} M_e \otimes M_e \otimes M_e,$$

where M_e is defined in (11). The symbol of M can be obtained by tensor product given by

$$\widetilde{M} = \frac{h^2}{27}(2 + \cos\theta_1)(2 + \cos\theta_2)(2 + \cos\theta_3).$$

The symbol of A_h in 3D is

$$\widetilde{A}_h = \frac{1}{h^2} 2(3 - \cos\theta_1 - \cos\theta_2 - \cos\theta_3).$$

Let $M_J = \frac{6}{h^2} I$, which is the Jacobi matrix. If we consider the point-wise damped Jacobi as a smoother for the Laplacian, then the corresponding optimal smoothing factor of $S = I - \omega M_J A_h$ is

$$\mu_{J,\text{opt}} = \min_{\omega} \max_{\theta \in T^{\text{high}}} |1 - \omega \widetilde{M}_J \widetilde{A}_h| = \frac{5}{7} \approx 0.714, \tag{31}$$

where the minimum is uniquely achieved at $\omega_{\text{opt}} = \frac{6}{7} \approx 0.857$. This result can be found in Trottenberg et al.[28] Next, we consider mass-based relaxation scheme for the Laplacian in 3D.

Theorem 6. Given the scaled mass stencil M in (3.3) and mass-based relaxation scheme $S_m = I - \omega M A_h$ in 3D, the corresponding optimal smoothing factor is

$$\mu_{m,\text{opt}} = \min_{\omega} \max_{\theta \in T^{\text{high}}} |1 - \omega \widetilde{M} \widetilde{A}_h| = \frac{131}{212} \approx 0.618, \tag{32}$$

where the minimum is uniquely achieved at $\omega = \omega_{opt} = \frac{729}{848} \approx 0.860$.

Proof. Let

$$\widetilde{M}\widetilde{A}_h = \frac{2}{27}(2 + \cos\theta_1)(2 + \cos\theta_2)(2 + \cos\theta_2)(3 - \cos\theta_1 - \cos\theta_2 - \cos\theta_3).$$

Define $g(x, y, z) = \frac{2}{27}(2 + x)(2 + y)(2 + z)(3 - x - y - z)$ with $x, y, z \in [-1, 1]$. To find the extremals of g, we will consider its derivatives and the function values at the boundary of underlying domain. We compute the

derivatives of g with respect to x, y, and z, given by

$$g_x = \frac{2}{27}(2+y)(2+z)(1-2x-y-z),$$
$$g_y = \frac{2}{27}(2+x)(2+z)(1-2y-x-z),$$
$$g_z = \frac{2}{27}(2+x)(2+y)(1-2z-x-y).$$

Solving $g_x = g_y = g_z = 0$ with $x, y, z \in [-1, 1]$ gives $x = y = z = 1/4$. However, $\boldsymbol{\theta}^* = (\theta_1, \theta_2, \theta_3)$ such that $(\cos\theta_1, \cos\theta_2, \cos\theta_3) = (1/4, 1/4, 1/4)$ does not belong to T^{high}.

Let us define $\Omega_1 = [-1, 1]^3$, $\Omega_2 = [0, 1]^3$, and $\Omega = \Omega_1 \setminus \Omega_2$. Note that Ω corresponds to $\boldsymbol{\theta} \in T^{\text{high}}$. To find the extremals of g for $\boldsymbol{\theta} \in T^{\text{high}}$, we only need to find the extremals of g at the boundary of Ω, denoted as $\partial\Omega$. Note that $\partial\Omega$ contains the following four cases.

Case 1:

$$x = -1, (y, z) \in [-1, 1]^2,$$
$$y = -1, (x, z) \in [-1, 1]^2,$$
$$z = -1, (x, y) \in [-1, 1]^2.$$

Case 2:

$$x = 1, (y, z) \in [-1, 0] \times [-1, 1],$$
$$y = 1, (x, z) \in [-1, 0] \times [-1, 1],$$
$$z = 1, (x, y) \in [-1, 0] \times [-1, 1].$$

Case 3:

$$x = 0, (y, z) \in [0, 1]^2,$$
$$y = 0, (x, z) \in [0, 1]^2$$
$$z = 0, (x, y) \in [0, 1]^2.$$

Case 4:

$$x = 1, (y, z) \in [0, 1] \times [-1, 0],$$
$$y = 1, (x, z) \in [0, 1] \times [-1, 0],$$
$$z = 1, (x, y) \in [0, 1] \times [-1, 0].$$

Due to the symmetry of $g(x, y, z)$ and our interest of maximum and minimum of $g(x, y, z)$, we only need to consider the following sets

$$\mathcal{D}_1 = \left\{(x, y, z) |\ x = -1, (y, z) \in [-1, 1]^2\right\},$$
$$\mathcal{D}_2 = \left\{(x, y, z) |\ x = 1, (y, z) \in [-1, 0] \times [-1, 1]\right\},$$
$$\mathcal{D}_3 = \left\{(x, y, z) |\ x = 0, (y, z) \in [0, 1]^2\right\},$$
$$\mathcal{D}_4 = \left\{(x, y, z) |\ x = 1, (y, z) \in [0, 1] \times [-1, 0]\right\}.$$

For $\boldsymbol{\theta} \in T^{\text{high}}$, we check the extremals of $g(x, y, z)$ on the sets $\mathcal{D}_1 \bigcup \mathcal{D}_2 \bigcup \mathcal{D}_3 \bigcup \mathcal{D}_4$, and find that the maximum of g is $\frac{4 \cdot 7^3}{3^6}$ achieved at $(\cos\theta_1, \cos\theta_2, \cos\theta_3) = (0, 1/3, 1/3)$ and the smallest value of g is $\frac{4}{9}$ with $(\cos\theta_1, \cos\theta_2, \cos\theta_3) = (-1, -1, -1)$. Thus, the optimal parameter is $\omega = \frac{2}{4/9 + 4 \cdot 7^3/3^6} = \frac{729}{848} \approx 0.860$ and the corresponding smoothing factor is $\mu_{m,\text{opt}} = 1 - \frac{729}{848}\frac{4}{9} = \frac{131}{212} \approx 0.618$. ■

Remark 2. One might consider a tensor-product generalization, that is, $h^{-4}M_v \otimes M_v \otimes M_v$, where M_v is defined in (15), as a smoother for the Laplacian in 3D. However, with this choice, we find that the numerically optimal smoothing factor is 0.800, which is larger than 0.618, see (32), obtained from the mass-based relaxation. Thus, we do not further explore this tensor product form.

For the smoothing analysis of Vanka-type smoothers, we need to solve the minmax problem (7) in 3D for $\boldsymbol{\theta}$ and ω. Obtaining an analytical solution for such a problem seems difficult or impossible, and we do not further pursue it.

4 | NUMERICAL EXPERIMENTS

We comment on the computational cost. In general, the Jacobi scheme is attractively simple and a single iteration is computationally cheap. For the mass-based and Vanka-type smoothers, our LFA allows us to derive the inverses of the smoothers explicitly, so that in the corresponding algorithms we apply matrix-vector products and avoid computing inverses. This presents significant computational savings and results in relatively cheap iterations. In our numerical experiments, implemented straightforwardly in a MATLAB environment, we observe that the Vanka scheme and mass scheme are slightly more efficient than Jacobi; see Section 4.2.

4.1 | LFA predictions

In this subsection we compute the smoothing factor to validate our theoretical results. We also report the LFA two-grid convergence factor and compare it to the corresponding smoothing factor.

In general, the two-grid error-propagation operator can be expressed as[1,2]

$$E = S^{\nu_2}(I - PA_H^{-1}RA_h)S^{\nu_1}, \tag{33}$$

where R is the restriction operator from grid h to grid H, P is the interpolation operator from grid H to grid h, A_H represents the coarse-grid operator, and the integers ν_1 and ν_2 are the numbers of pre- and post-relaxation sweeps, respectively. Here, S is the relaxation error operator defined in (6).

Definition 3. The LFA two-grid convergence factor[28,29] for E is defined as

$$\rho = \max_{\boldsymbol{\theta}\in T^{\text{low}}} \left\{ \rho(\widetilde{E}(\boldsymbol{\theta},\omega)) \right\}, \tag{34}$$

where ω is a parameter, $\widetilde{E}$ denotes the symbol of the two-grid error operator E, and $\rho(\widetilde{E}(\boldsymbol{\theta},\omega))$ denotes the spectral radius of the matrix $\widetilde{E}$.

In our tests, we consider P to be the standard (bi)linear interpolation and take $R = cP^T$, where $c = 2^{-d}$ and d is the dimension, and $A_H = RA_hP$. We take ρ to be the LFA prediction sampled at 64 equispaced points in each dimension of the Fourier domain. For simplicity, we denote by $T(\nu)$ the two-grid method with $\nu = \nu_1 + \nu_2$.

In Figure 2, we present the eigenvalue distribution of $\widetilde{E}$ for the Vanka-type method in 2D with the optimal value of ω. We see that all eigenvalues of $\widetilde{E}$ are real and their largest magnitude matches the optimal smoothing factor.

Figure 3 shows the magnitude of eigenvalues of $\widetilde{E}_e$ and $\widetilde{S}_v$ as a function of the Fourier modes, (θ_1, θ_2), in 2D. We see that the eigenvalues of the two-grid error operator are distributed almost evenly in the entire Fourier domain. On the other hand, for the vertex-wise Vanka, the largest magnitude occurs at $(0, \pm\pi)$ or $(\pm\pi, 0)$, see Figure 4. The plots on the right in Figures 3 and 4 show that the smoother reduces the high frequency errors rather rapidly. The (experimental) value of μ_{opt} validates our analytical result for the smoothing factor.

From Table 2, we see that the smoothing factors match the two-grid convergence factor with $\nu = 1$ (except for the vertex-wise patch for 1D), which is as expected since the smoothing factor typically offers a sharp prediction of the two-grid convergence factor. As ν increases, we see a little degradation of $\rho(\nu)$, that is $\rho(\nu) > \mu^\nu$ for Vanka-type relaxation, and so does the mass-based relaxation scheme with $\nu = 4$.

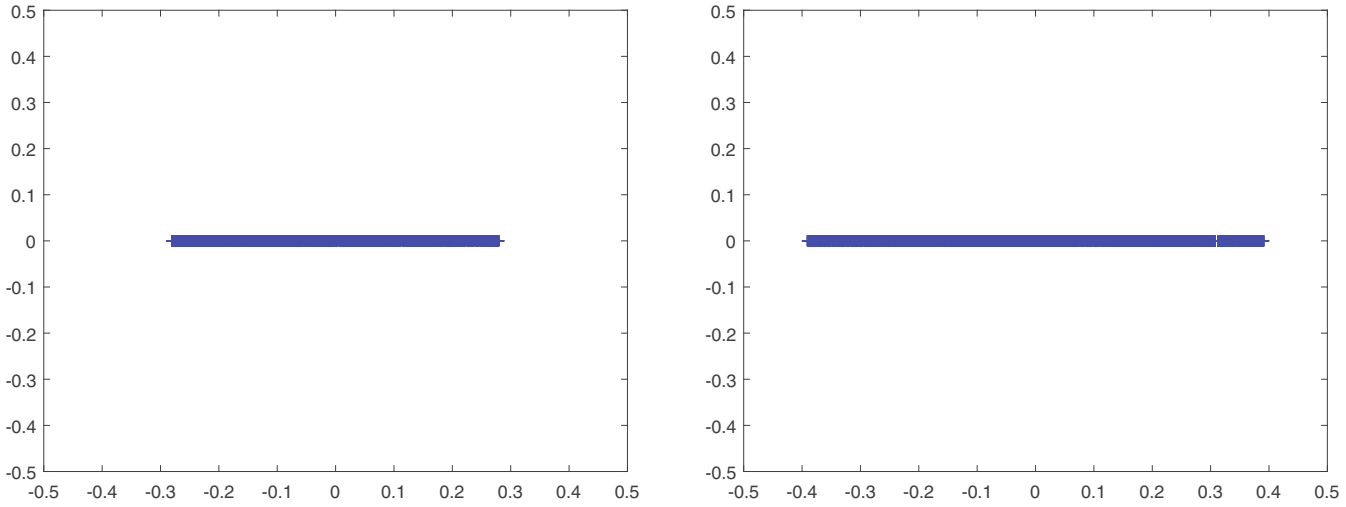

FIGURE 2 Eigenvalue distribution of $\widetilde{E}$ for Vanka-type method with $\nu = 1$. Left: Element-wise Vanka. Right: Vertex-wise Vanka.

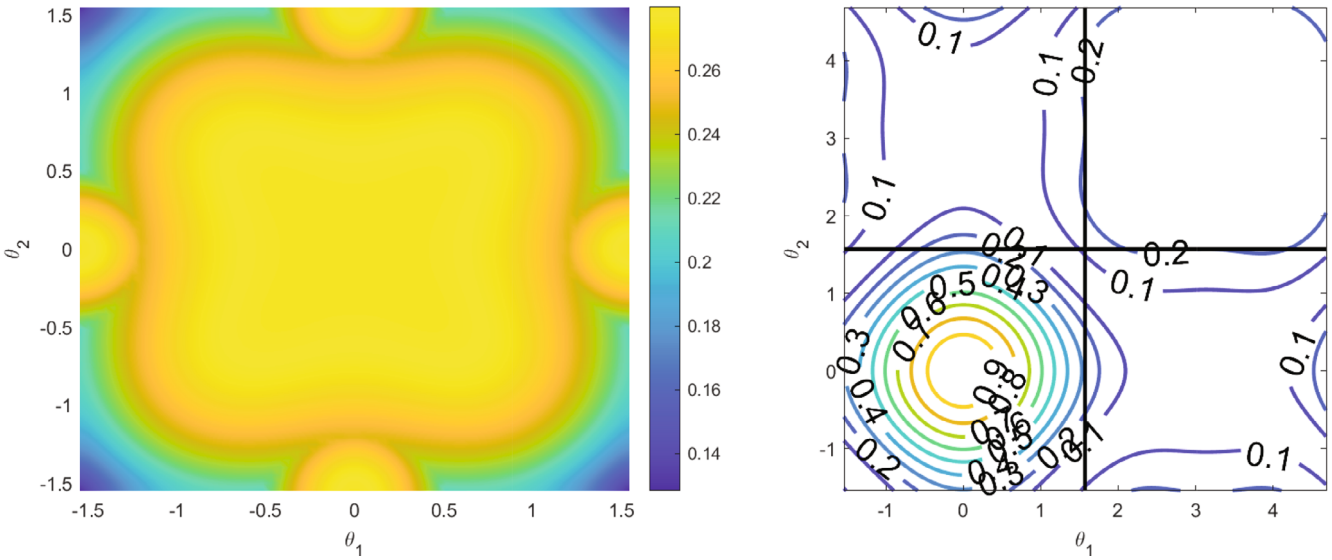

FIGURE 3 Element-wise Vanka with $\nu = 1$. Left: The magnitude of eigenvalues of $\widetilde{E}_e$ as a function of the Fourier modes, (θ_1, θ_2). Right: The magnitude of eigenvalues of $\widetilde{S}_e$ as a function of the Fourier modes, (θ_1, θ_2).

For the 2D problem, the smoothing factor of GS-RB is 0.25,[28] which is close to our element-wise Vanka smoothing factor of 0.28. For 3D, GS-RB has a smoothing factor of 0.44, which is superior to our mass smoothing factor of 0.62. We speculate that the gap is smaller for Vanka-type smoothing; we have not pursued this.

To compare the optimal smoothing factor with the optimal LFA two-grid convergence factor, we run our LFA code to minimize the LFA two-grid convergence factor for $\nu = 1$ with respect to ω by an exhaustive search with stepsize 0.01 and $h = 1/64$. Denote the corresponding optimal ω as ω^*. Table 3 shows the LFA predictions with $\omega = \omega^*$. We have found that in both the 2D and 3D cases the optimal smoothing factor is equal to the optimal LFA two-grid convergence factor. For the vertex-wise Vanka in 1D, the gap between the LFA two-grid convergence factor with $\nu = 1$ and the smoothing factor is reasonable, because the LFA two-grid convergence factor accounts for the effect of coarse-grid correction as well as smoothing. However, for $\nu > 1$, using ω^* and ω_{opt} leads to same LFA two-grid convergence factor. For the element-wise Vanka in 1D, optimizing the LFA two-grid convergence factor with $\nu = 1$ gives a very small two-grid convergence factor compared with the optimal smoothing factor. Again, for $\nu > 1$, using ω^* and ω_{opt} leads to almost the same convergence factors.

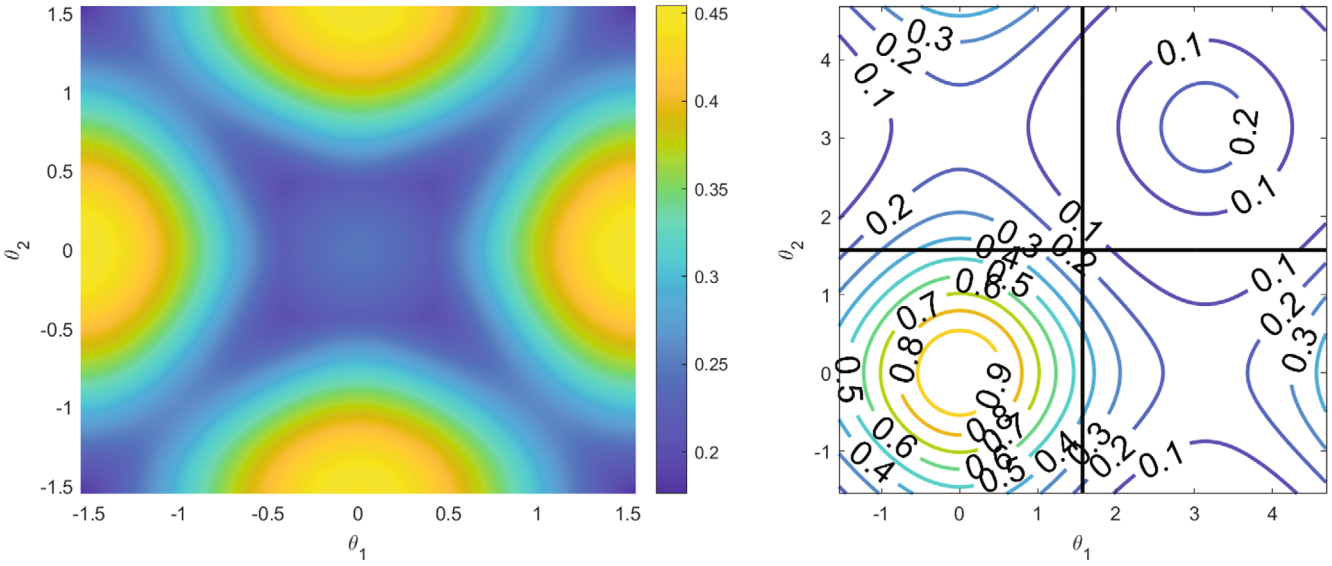

FIGURE 4 Vertex-wise Vanka with $\nu = 1$. Left: The magnitude of eigenvalues of $\widetilde{E}_v$ as a function of the Fourier modes, (θ_1, θ_2). Right: The magnitude of eigenvalues of $\widetilde{S}_v$ as a function of the Fourier modes, (θ_1, θ_2).

TABLE 2 LFA prediction: ω_{opt} is obtained from our analytical result and $h = \frac{1}{64}$.

Cycle	ω_{opt}	μ_{opt}	$TG(1)$	$TG(2)$	$TG(3)$	$TG(4)$
1D						
ρ_e	12/17	0.059	0.059	0.059	0.040	0.031
ρ_v	81/104	0.038	0.091	0.033	0.022	0.017
2D						
ρ_e	24/25	0.280	0.280	0.092	0.059	0.045
ρ_v	20/23	0.391	0.391	0.153	0.076	0.055
ρ_{fe}	3/4	0.333	0.333	0.111	0.037	0.029
3D						
ρ_J	6/7	0.714	0.714	0.510	0.364	0.260
ρ_m	729/848	0.618	0.618	0.382	0.236	0.146

Remark 3. The LFA two-grid convergence and smoothing factors seem independent of the meshsize h. We have tested different values of h for Table 2 to confirm this. Further details are omitted.

4.2 | Multigrid performance

In this section, we report multigrid performance for the 2D and 3D Poisson problems defined on the domains $[0,1]^2$ and $[0,1]^3$, respectively. We set up the problems so that the analytical solutions are given by $u(x,y) = \sin(\pi x)\sin(\pi y)$ and $u(x,y,z) = \sin(\pi x)\sin(\pi y)\sin(\pi z)$, respectively. To confirm our LFA predictions, we report the results of W-cycle multigrid, where we use one pre-smoothing relaxation and no post-smoothing relaxation. The coarsest grid has four cells in each direction and the finest grid has $n = 256$ cells in each direction. For our tests, we have used an open-source MATLAB code, available at https://github.com/junliu2050/SPAI-MG-Laplacian. The stopping criterion is $\|r_k\|_2 \le 10^{-10}\|r_0\|_2$, where $r_k = b_h - A_h x^k$ with x^k being the kth multigrid approximation. For generating Kronecker products for the three-dimensional problem, we have used an efficient open-source MATLAB code.[31]

TABLE 3 LFA prediction: ω^* is obtained from numerically optimizing LFA two-grid convergence factor with $\nu = 1$, and $h = \frac{1}{64}$.

Cycle	ω^*	μ	$TG(1)$	$TG(2)$	$TG(3)$	$TG(4)$
1D						
ρ_e	0.75	0.125	3e-09	0.062	0.037	0.029
ρ_v	0.80	0.067	0.066	0.031	0.022	0.016
2D						
ρ_e	0.96	0.280	0.280	0.092	0.059	0.045
ρ_v	0.87	0.392	0.392	0.154	0.076	0.055
ρ_{fe}	0.75	0.331	0.331	0.111	0.037	0.029
3D						
ρ_J	0.85	0.710	0.716	0.513	0.368	0.263
ρ_m	0.86	0.618	0.618	0.382	0.236	0.146

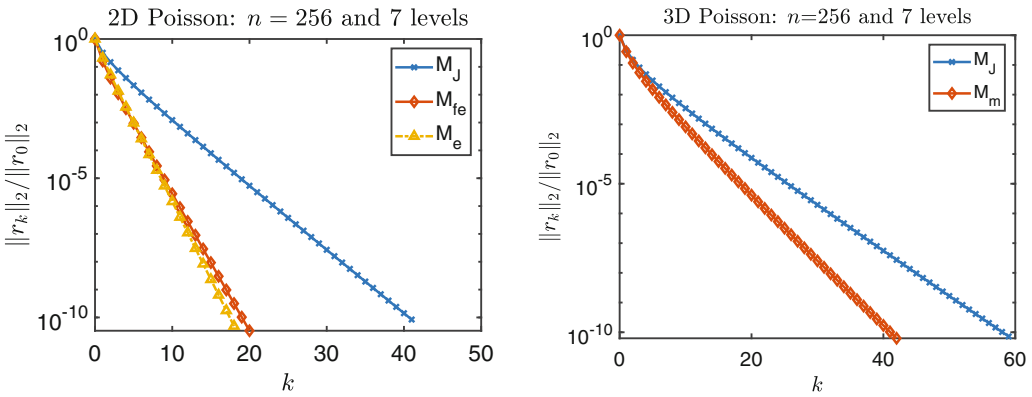

FIGURE 5 Left: Multigrid convergence history for 2D; Right: Multigrid convergence history for 3D.

In Figure 5, we report W-cycle multigrid convergence history. As per the discussion thus far, for 2D we show the results related to element-wise Vanka and mass smoothing, whereas for 3D we only show the results of mass smoothing. We compare those results to damped Jacobi. We see that in 2D there is no significant difference between the Vanka smoothing and the mass smoothing, and both converge within approximately a half of the iteration count of Jacobi. In 3D, the mass smoothing scheme takes approximately two thirds of the iteration count of Jacobi. Those results are consistent with our LFA predictions.

We add the following information about the multigrid results given in Figure 5. We have run one hundred experiments with random initial guesses for each of the 2D and the 3D problems, and are reporting the average running times. For 2D, multigrid with Jacobi takes an average of 0.19 s, multigrid with mass smoothing takes 0.15 seconds, and multigrid with element-wise Vanka takes 0.14 s. In 3D, multigrid with Jacobi takes 59.34 s on average and multigrid with mass smoothing takes 55.49 s. This indicates that the proposed new schemes are potentially efficient and may be advantageous especially for complicated problems.

5 | CONCLUSIONS

We have presented a theoretical analysis of the optimal multigrid smoothing factor for two types of additive Vanka smoothers, applied to the Poisson equation discretized by the standard centered finite difference scheme. The smoothers are shown to have a fast convergence rate. We have found that element-wise Vanka can be expressed as a linear combination of the mass matrix obtained from the (bi)linear finite element method and a scaled identity. This observation has led us to explore using the mass matrix as a smoother. Solvers for equations related to the Laplacian are a natural first step

in developing new algorithms for more complex problems, such as the Stokes equations, Navier–Stokes equations and other saddle-point problems. Exploring a similar approach as part of the development of fast solvers for those problems may prove computationally beneficial.

ACKNOWLEDGMENTS

We are grateful to two anonymous referees for their helpful comments.

CONFLICT OF INTEREST STATEMENT

The authors declare no potential conflict of interests.

DATA AVAILABILITY STATEMENT

Data sharing is not applicable to this article as no new data were created or analyzed in this study.

REFERENCES

1. Stüben K, Trottenberg U. Multigrid methods: Fundamental algorithms, model problem analysis and applications. In: Hackbusch W, Trottenberg U, editors. Multigrid methods. Berlin: Springer; 1982. p. 1–176.
2. Wesseling P. An introduction to multigrid methods. Pure and applied mathematics. Chichester: John Wiley & Sons, Ltd; 1992.
3. Yavneh I. Multigrid smoothing factors for red-black Gauss–Seidel relaxation applied to a class of elliptic operators. SIAM J Numer Anal. 1995;32(4):1126–38.
4. Kuo CCJ, Levy BC. Two-color Fourier analysis of the multigrid method with red-black Gauss-Seidel smoothing. Appl Math Comput. 1989;29(1):69–87.
5. Yavneh I. On red-black SOR smoothing in multigrid. SIAM J Sci Comput. 1996;17(1):180–92.
6. Hocking LR, Greif C. Closed-form multigrid smoothing factors for lexicographic Gauss–Seidel. IMA J Numer Anal. 2012;32(3):795–812.
7. Zhang J. Acceleration of five-point red-black Gauss-Seidel in multigrid for Poisson equation. Appl Math Comput. 1996;80(1):73–93.
8. John V. Higher order finite element methods and multigrid solvers in a benchmark problem for the 3D Navier–Stokes equations. Int J Numer Methods Fluids. 2002;40(6):775–98.
9. Manservisi S. Numerical analysis of Vanka-type solvers for steady Stokes and Navier-Stokes flows. SIAM J Numer Anal. 2006;44(5):2025–56.
10. Vanka SP. Block-implicit multigrid solution of Navier-Stokes equations in primitive variables. J Comput Phys. 1986;65:138–58.
11. He Y, Rhebergen S, De Sterck H. Local Fourier analysis of multigrid for hybridized and embedded discontinuous Galerkin methods. SIAM J Sci Comput. 2021;43(5):S612–36.
12. Farrell PE, He Y, MacLachlan SP. A local Fourier analysis of additive Vanka relaxation for the Stokes equations. Numer Linear Algebra Appl. 2021;28(3):e2306.
13. Voronin A, He Y, MacLachlan S, Olson LN, Tuminaro R. Low-order preconditioning of the Stokes equations. Numer Linear Algebra Appl. 2022;29(3):e2426.
14. Adler JH, He Y, Hu X, MacLachlan S, Ohm P. Monolithic multigrid for a reduced-quadrature discretization of poroelasticity. SIAM J Sci Comput. 2022;S54–81.
15. Saberi S, Meschke G, Vogel A. A restricted additive Vanka smoother for geometric multigrid. J Comput Phys. 2022;459:111123.
16. Claus L, Bolten M. Nonoverlapping block smoothers for the Stokes equations. Numer Linear Algebra Appl. 2021;28:e2389.
17. de la Riva AP, Rodrigo C, Gaspar FJ. A robust multigrid solver for Isogeometric analysis based on multiplicative Schwarz smoothers. SIAM J Sci Comput. 2019;41(5):S321–45.
18. de la Riva ÁP, Rodrigo C, Gaspar FJ. A two-level method for isogeometric discretizations based on multiplicative Schwarz iterations. Comput Math Appl. 2021;100:41–50.
19. Franco S, Rodrigo C, Gaspar F, Pinto M. A multigrid waveform relaxation method for solving the poroelasticity equations. Comput Appl Math. 2018;37:4805–20.
20. Adler JH, Benson TR, MacLachlan SP. Preconditioning a mass-conserving discontinuous Galerkin discretization of the Stokes equations. Numer Linear Algebra Appl. 2017;24(3):e2047.
21. John V, Tobiska L. Numerical performance of smoothers in coupled multigrid methods for the parallel solution of the incompressible Navier-Stokes equations. Int J Numer Methods Fluids. 2000;33(4):453–73.
22. Molenaar J. A two-grid analysis of the combination of mixed finite elements and Vanka-type relaxation. In: Hackbusch W, Trottenberg U, editors. Multigrid Methods III. Berlin: Springer; 1991. p. 313–23.
23. Frommer A, Szyld DB. Weighted max norms, splittings, and overlapping additive Schwarz iterations. Numer Math. 1999;83(2):259–78.
24. MacLachlan SP, Oosterlee CW. Local Fourier analysis for multigrid with overlapping smoothers applied to systems of PDEs. Numer Linear Algebra Appl. 2011;18(4):751–74.
25. Wobker H, Turek S. Numerical studies of Vanka-type smoothers in computational solid mechanics. Adv Appl Math Mech. 2009;1(1):29–55.
26. Adler JH, Benson TR, Cyr EC, MacLachlan SP, Tuminaro RS. Monolithic multigrid methods for two-dimensional resistive magnetohydrodynamics. SIAM J Sci Comput. 2016;38(1):B1–B24.
27. Brubeck PD, Farrell PE. A scalable and robust vertex-star relaxation for high-order FEM, arXiv preprint arXiv:210714758; 2021.

28. Trottenberg U, Oosterlee CW, Schüller A. Multigrid. San Diego, CA: Academic Press, Inc; 2001.
29. Wienands R, Joppich W. Practical Fourier analysis for multigrid methods. Boca Raton, FL: CRC Press; 2004.
30. Strang G, Fix GJ. An analysis of the finite element method. Hoboken, NJ: Prentice Hall; 1973.
31. Matt J. Efficient object-oriented Kronecker product manipulation. Available from. https://www.mathworks.com/matlabcentral/fileexchange/25969-efficient-object-oriented-kronecker-product-manipulation

How to cite this article: Greif C, He Y. A closed-form multigrid smoothing factor for an additive Vanka-type smoother applied to the Poisson equation. Numer Linear Algebra Appl. 2023;30(5):e2500. https://doi.org/10.1002/nla.2500